Charge-Noise Resilience of Two-Electron Quantum Dots in Si/SiGe Heterostructures

H. Ekmel Ercan,[1] Mark Friesen,[1] and S. N. Coppersmith[1,2]
[1]Department of Physics, University of Wisconsin-Madison, Madison, Wisconsin 53706, USA
[2]School of Physics, The University of New South Wales, Sydney, New South Wales 2052, Australia

(Received 3 June 2021; revised 30 March 2022; accepted 7 April 2022; published 16 June 2022)

The valley degree of freedom presents challenges and opportunities for silicon spin qubits. An important consideration for singlet-triplet states is the presence of two distinct triplets, composed of valley vs orbital excitations. Here, we show that both of these triplets are present in the typical operating regime, but that only the valley-excited triplet offers intrinsic protection against charge noise. We further show that this protection arises naturally in dots with stronger confinement. These results reveal an inherent advantage for silicon-based multielectron qubits.

DOI: 10.1103/PhysRevLett.128.247701

When quantum dots contain more than one electron, new possibilities emerge for defining and controlling qubits. Theoretical studies have shown that GaAs dots with multiple electrons may be inherently protected from charge noise [1–3], and recent experiments confirm some of these predictions [4–6]. Recent progress in Si-based multielectron qubits [7–12] brings renewed attention to such noise-reduction schemes. However, the theoretical description of GaAs dots is not applicable to Si, due to the presence of both orbital and valley degrees of freedom for the electrons. While the orbital energies are determined by electrostatic confinement, similar to GaAs, the conduction-band valley splitting is determined by details of the quantum-well interface [13]. It is technically challenging to describe such behavior because of the strong electron-electron (e-e) interactions that must be treated nonperturbatively, and because a minimal model of Si must include details of the Si band structure, as well as atomic-scale disorder at the quantum well interface, which gives rise to valley-orbit coupling (VOC) [14].

Here, we develop a complete theoretical toolbox for describing two-electron dots in Si. We first apply these tools to study low-energy spin singlet and triplet states. Solving the two-electron wave functions as a function of orbital confinement energy $E_{\rm orb} \sim \hbar\omega$ reveals two fundamentally different triplet excitations, based on their valley or orbital character, as illustrated in Figs. 1(a)–1(c). These excitations also have different coherence properties. For small $\hbar\omega$, the low-energy states that define the qubit are the singlet (S) and orbital triplet ($T_{\rm orb}$). Since these states have dissimilar charge distributions, they couple differently to electrical fluctuations [e.g., a nearby charge trap (CT), as shown in Fig. 1(d)], resulting in dephasing. For stronger confinement (larger $\hbar\omega$), the low-energy states are S and the valley triplet ($T_{\rm val}$). In this case, the charge distributions are very similar, and they respond similarly to electrical fluctuations [Fig. 1(e)], yielding qubits that are resilient to dephasing. These results obtained below are applicable to any two-electron dot system, and are especially relevant for quantum dot hybrid qubits (QDHQs) [7,8], in which the qubit energy is largely determined by the ST splitting of two electrons in a single dot. Double occupation of a single dot also defines the "parking" regime of a singlet-triplet qubit, which may be used to suppress the effects of decoherence or crosstalk [15].

Theoretical methods.—We compute two-electron wave functions in two steps. First, we use a tight-binding (TB) approach to obtain single-electron wave functions [16,17]. This method accounts for the essential features of the Si band structure and allows an atomistic description of disorder at the quantum well interface. Second, we incorporate these single-electron wave functions into a full configuration interaction (FCI) [18] scheme for computing two-electron wave functions, nonperturbatively, while accounting for strongly interacting electrons. The full method is summarized in Fig. 2; additional details are given in Ref. [19].

In step one, the single-electron Hamiltonian for the 3D heterostructure is assumed to be separable in terms of the (x, z) vs y variables, where $\hat{x}$, $\hat{y}$, and $\hat{z}$ are the crystallographic axes. We consider atomistic disorder only in the x-z plane. This simplification allows us to treat the (x, z) variables using TB methods, while solving the separable y wave functions using continuum effective-mass theory, which allows us to achieve full convergence on a more practical timescale. The single-electron Hamiltonian can then be written as

$$H^{1e} = H_K + H_E + H_{\rm QW}. \tag{1}$$

Here, the kinetic energy is given by

$$H_K = \frac{-\hbar^2}{2m_t}\frac{\partial^2}{\partial y^2} + \sum_{i_x,i_z}(t_1|i_x, i_z+1\rangle\langle i_x, i_z| + t_2|i_x, i_z+2\rangle\langle i_x, i_z| + t_3|i_x+1, i_z\rangle\langle i_x, i_z| + \text{H.c.}), \tag{2}$$

 © 2022 American Physical Society

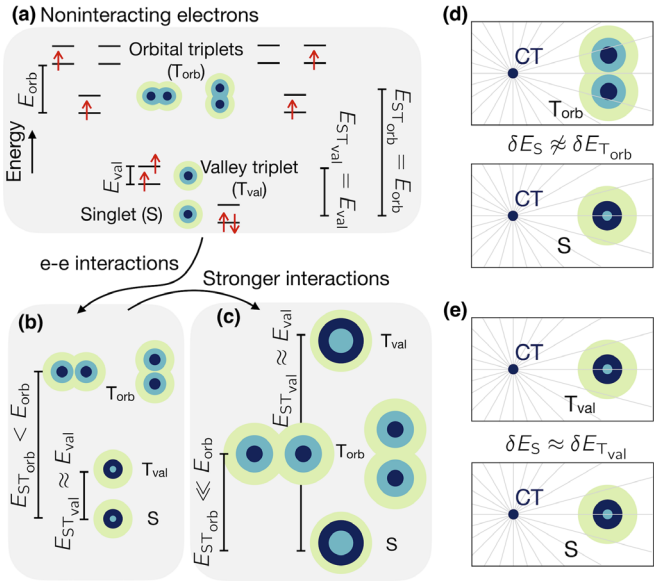

FIG. 1. Effects of e-e interactions and electrical noise on singlet-triplet states in a two-electron Si/SiGe quantum dot. (a) Noninteracting electrons. Single-electron energy levels (black lines) include valley and orbital excited states, with $E_{\mathrm{val}} < E_{\mathrm{orb}}$. Two-electron states ($S$, T_{val}, and T_{orb}) are formed from combinations of spin, valley, and orbital states (red arrows). Charge distributions are shown schematically, with darker colors indicating higher densities. The two T_{orb} states have distinct p_x or p_y character. (b) Including e-e interactions. In the high-E_{orb} regime, we find $E_{ST_{\mathrm{val}}} < E_{ST_{\mathrm{orb}}}$. The resulting low-energy states (S and T_{val}) have very similar charge distributions. (c) Stronger e-e interactions (low-E_{orb} regime). Here, $E_{ST_{\mathrm{orb}}} < E_{ST_{\mathrm{val}}}$, and the low-energy states (S and T_{orb}) have very different charge distributions. (d),(e) The responses of S, T_{orb}, and T_{val} to a charge trap (CT) depend on their charge distributions. (d) Dissimilar distributions give large $E_{ST_{\mathrm{orb}}}$ fluctuations. (e) Similar distributions give small $E_{ST_{\mathrm{val}}}$ fluctuations.

where the integer indices i_x and i_z refer to TB sites along the $\hat{x}$ and $\hat{z}$ axes, respectively. We have suppressed the spin index here, because our Hamiltonian is independent of spin, and the effects of Pauli exclusion become important only at the FCI stage of the calculation. The hopping parameters $t_1 = 0.68$ eV and $t_2 = 0.61$ eV are chosen to reproduce the key features of the twofold degenerate structure at the bottom of the Si conduction band: (1) valleys centered at $\mathbf{k} = \pm k_0 \hat{z}$ in reciprocal space, where $k_0 = \pm 0.82(2\pi/a)$, $a = 5.43$ Å is the cubic lattice constant, and $\Delta z = a/4$ is the grid spacing, and (2) longitudinal effective mass, $m_l = 0.916 m_0$. The hopping parameter $t_3 = -0.026$ eV gives the correct transversal effective mass, $m_t = 0.191 m_0$, for the grid spacing $\Delta x = 2.79$ nm [20]. We note that Δx can be much larger than Δz, because there are no fast valley oscillations along $\hat{x}$. The vertical (quantum well) confinement potential is given by

$$H_{\mathrm{QW}} = \sum_{i_x,i_z} [E_0 + V_{\mathrm{QW}}\Theta_{i_x,i_z} - e(i_x F_x^e \Delta x + i_z F_z^e \Delta z)]|i_x, i_z\rangle\langle i_x, i_z|, \quad (3)$$

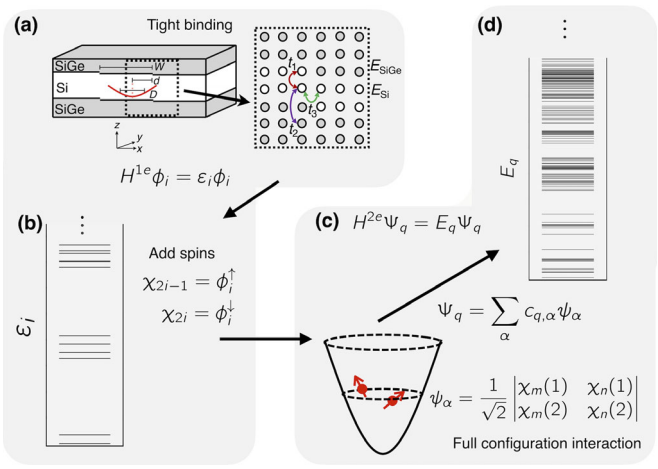

FIG. 2. Overview of theoretical methods. (a) Schematic of the 2D TB method used to compute single-electron wave functions, while accounting for atomic-scale disorder at the quantum well interface. Si sites are shown as white and SiGe sites are shown as gray. Interface steps have width W, the harmonic dot confinement potential (red) has diameter D, and we take the dot to be centered halfway between two steps, $d = W/2$. Hopping parameters t_1, t_2, and t_3 and on-site parameters are discussed in the main text. (b) Typical results for single-electron energies ε_i. (c) FCI step: Slater determinants ψ_α are computed for spin orbitals χ_i, obtained from TB valley orbitals ϕ_i, combined with spin coordinates. The two-electron Hamiltonian H^{2e} is diagonalized in this Slater basis, with enough spin-orbit basis states (84) to ensure convergence. (d) Typical results for two-electron energies E_q.

where Θ_{i_x,i_z} is a step function that takes the value 1 on a SiGe site and 0 on a Si site, $V_{\mathrm{QW}} = 150$ meV is the band offset between Si and SiGe, $e = |e|$ is the elementary charge, and $\boldsymbol{F}^e = (F_x^e, 0, F_z^e)$ is the electric field perpendicular to the interface due to the gate electrodes. All calculations assume 10 nm quantum wells. Interface disorder is implemented via the choice of Θ_{i_x,i_z}. In this Letter, we consider an interface tilted slightly away from $\hat{z}$, with uniformly distributed single-atom steps of height $a/4$ and width W, as depicted in Fig. 2(a). The field $\boldsymbol{F}^e$ is taken to be perpendicular to the tilted interface. The lateral confinement potential is of electrostatic origin, and is taken to be parabolic [21], with the form

$$H_E = \frac{1}{2} m_t \omega_x^2 \sum_{i_x,i_z} (i_x \Delta x)^2 |i_x, i_z\rangle\langle i_x, i_z| + \frac{1}{2} m_t \omega_y^2 y^2. \quad (4)$$

We solve $H^{1e}\phi_i = \varepsilon_i\phi_i$ to obtain the single-electron basis states ϕ_i used in the FCI calculation. A typical energy level structure is shown in Fig. 2(b).

In step two, we solve the two-electron Hamiltonian, which includes the Coulomb interaction term

$$H^{2e} = H^{1e}(\boldsymbol{r}_1) + H^{1e}(\boldsymbol{r}_2) + \frac{e^2}{4\pi\epsilon_0\epsilon_r} \frac{1}{|\boldsymbol{r}_1 - \boldsymbol{r}_2|}, \quad (5)$$

where ϵ_0 is the permittivity of free space, and $\epsilon_r = 11.4$ is the dielectric constant of low-temperature Si [24]. The Coulomb matrix elements are computed using a combination of numerical and analytical methods, taking advantage of the analytical wave function solutions along $\hat{y}$. We then solve for the eigenvalues and eigenstates of $H^{2e}\Psi_q = E_q\Psi_q$ using FCI methods: H^{2e} is diagonalized in a basis of Slater determinants generated from spin orbitals $\chi = \phi \otimes \uparrow$ or $\chi = \phi \otimes \downarrow$, as shown in Figs. 2(c) and 2(d). A finite set of determinants is used and the convergence of the FCI method is checked, as in Ref. [19]. Finally, we note that spin-orbit interactions and external magnetic fields have been ignored in this Letter, since the former are expected to be much weaker than valley-orbit interactions in Si/SiGe heterostructures, while the latter are not required for operating QDHQs [19].

Results.—To better understand the nontrivial behavior arising from *e-e* interactions and VOC, it is instructive to consider these effects one at a time, as summarized in Fig. 1. In the absence of interactions, the ground-state singlet (S) is formed from two electrons, each in the lowest orbital level. There are two different types of single-electron excitations above the ground state: valleys and orbitals, with corresponding single-electron excitation energies, E_{val} and E_{orb}. Two-electron excitations take on the character of these single-electron excitations, yielding distinct valley (T_{val}) and orbital (T_{orb}) triplets, with excitation energies $E_{ST_{\mathrm{val}}} = E_{\mathrm{val}}$ and $E_{ST_{\mathrm{orb}}} = E_{\mathrm{orb}}$. Here, we assume $E_{\mathrm{val}} < E_{\mathrm{orb}}$, as consistent with many qubit experiments [25–31]. The charge distribution of T_{val} is identical to S; however T_{orb} is quite different, due to its p-orbital contribution. Now, introducing *e-e* interactions [Fig. 1(b)], we find that many additional Slater determinants contribute to the two-electron wave functions. To a very good approximation, the triplets retain their valley or orbital character; however the *e-e* interactions strongly suppress $E_{ST_{\mathrm{orb}}}$ below E_{orb}, while having almost no effect on $E_{ST_{\mathrm{val}}} \approx E_{\mathrm{val}}$ [19]. The charge distributions for S and T_{val} take the form of Wigner-molecule doughnuts, with dimples at their centers [32–36]. For stronger interactions [i.e., smaller $\hbar\omega$, Fig. 1(c)], there is a crossover from T_{val} to T_{orb}-dominated excitations. In this regime, the qubit states (S and T_{orb}) have very different charge distributions.

We finally consider a realistic dot model including *e-e* interactions and VOC. Typical results for excitation energies are shown in Fig. 3(a). To begin, we consider wide steps, $W = 101$ nm, to clearly demonstrate the types of behavior observed as a function of $\hbar\omega$. We also position the dot as far as possible from a step, with $d = W/2$, as depicted in Fig. 2(a). For small $\hbar\omega$ (weak confinement), T_{orb} is the dominant excitation, with an excitation energy, $E_{ST_{\mathrm{orb}}} \lesssim k_B T$, that is typically too small to enable high fidelity qubit initialization or readout. For larger $\hbar\omega > 600$ μeV, there is a crossover to T_{val}-dominated behavior. If the valley splitting is also $\gtrsim 100$ μeV, the energy $E_{ST_{\mathrm{val}}}$ will certainly be large enough for practical applications. (For quantum-dot QDHQs, slightly smaller E_{ST} are preferred [7,8].) For this calculation, we used $|\boldsymbol{F}^e| = 0.6$ MV/m. This particular value yields a valley splitting of $E_{\mathrm{val}} \sim 105$ μeV, as consistent with recent experiments [28]. We note that both electric field and disorder profiles play an important role in determining E_{ST} in actual devices, although neither can be well characterized. Rather than focus on such details here, we simply report our results for a fixed field value. However, we have confirmed that variations in the electric field do not qualitatively affect our main results. For $\hbar\omega$ values below the triplet crossover, $E_{ST_{\mathrm{val}}}$ drops quickly, as the dot (with diameter $D = 2\sqrt{\hbar/m_t\omega}$) begins to strongly overlap with different interface steps, suppressing the valley splitting [13], and causing VOC [14]. We can also explore other regimes by computing the excitation energies as a function of $\hbar\omega$ while holding $W = 2D$ fixed, as shown in Fig. 3(b), to ensure that the dot does not interact excessively with the steps. (This requires simultaneously changing W as $\hbar\omega$ is varied.) Here, we again observe a crossover from T_{orb} to T_{val}-dominated behavior. However, because the wave function remains far from the nearest step, $E_{ST_{\mathrm{val}}}$ is not suppressed for low $\hbar\omega$. In contrast, the insets of Fig. 3(b) show that smaller W/D ratios cause significant reductions in ST splittings, making it more difficult to achieve acceptable values for qubit applications. In Ref. [37] we further discuss interface profiles that give small ST splittings.

The crossover from T_{orb} to T_{val}-dominated behavior has a strong effect on qubit coherence, because the T_{orb} and T_{val} charge distributions couple differently to charge fluctuations. Previous work has considered the exploitation of the valley degree of freedom for protecting quantum information from environmental noise [38,39]; here, we specifically focus on the effects of charge noise on the ST energy splitting of a two-electron quantum dot, assuming realistic disorder and confinement models. For the QDHQ, for example, E_{ST} determines the qubit energy, and fluctuations of E_{ST} lead directly to dephasing [40]. The insets of Fig. 3(a) show typical in-plane electron densities for $\hbar\omega = 550$ and 650 μeV, which bracket the crossover between low-energy triplet states. As noted above, the charge distribution of S is very similar to that of T_{val} but not T_{orb}. These distinctions are still valid when the VOC, which mixes the valley and orbital character of the wave functions, is weak but nonzero. Consequently, charge noise affects S and T_{val} similarly, yielding weak fluctuations of $E_{ST_{\mathrm{val}}}$, but much larger fluctuations of $E_{ST_{\mathrm{orb}}}$. The high-$\hbar\omega$ regime is therefore expected to yield qubits with much better coherence properties.

To quantify these claims, we consider the effect of a charge trap, as depicted in Figs. 1(d) and 1(e). First-order perturbation theory is used to estimate the shifts in E_{ST} due to the electrostatic potential V_{CT} of the trap [2,3,41],

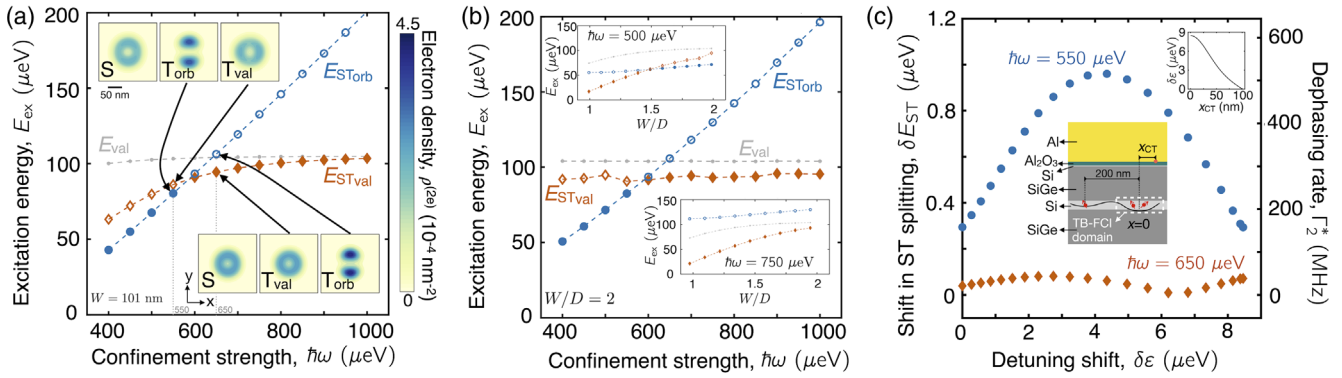

FIG. 3. Effects of $e-e$ interactions, interface steps, and a charge trap on the excitation energies of a two-electron dot. Solid symbols refer to the lowest ST excitation, which defines the qubit, and open symbols refer to the higher ST excitation. (a) ST splittings for fixed terrace width, $W = 101$ nm, with the dot center equidistant between two steps. [See Fig. 2(a) for device geometry.] The single-electron valley splitting $E_{\rm val}$ is also shown. $E_{ST_{\rm orb}}$ is strongly suppressed below $E_{\rm orb}$ (not shown) over its entire range, due to strong e-e interactions. A crossover is observed between regions dominated by $ST_{\rm orb}$ vs $ST_{\rm val}$. Here, $E_{ST_{\rm orb}}$ is typically too small to form practical qubits in the small-$\hbar\omega$ regime. Insets: charge densities of S, $T_{\rm orb}$, and $T_{\rm val}$ states, for two different confinement strengths. (b) ST splittings for fixed $W/D = 2$, where the dot diameter D depends on $\hbar\omega$ (so W also depends on $\hbar\omega$). Here, $E_{ST_{\rm val}} \approx E_{\rm val}$ is approximately constant, indicating that VOC is mainly determined by the overlap of the wave functions with interface steps. Insets: the same quantities are plotted as a function of W/D for fixed $\hbar\omega$, showing that $E_{ST_{\rm val}}$ is more strongly affected by the steps than $E_{ST_{\rm orb}}$. In (a) and (b), the triplet crossover occurs in an experimentally relevant regime. (c) Shift in E_{ST}, and corresponding qubit dephasing rate Γ_2^*, as a function of the shift in detuning, ε, due to the occupation of a charge trap near the top gate. Results are only shown for the low-lying excitations, just below or above the triplet crossover in (a). Γ_2^* is significantly lower for qubits defined by $T_{\rm val}$ since S and $T_{\rm val}$ have nearly identical charge distributions. Lower inset: schematic of the full double-dot geometry, with the smaller FCI simulation domain indicated. Upper inset: shift of the detuning ε of a double dot, for dots separated by 200 nm, due to the occupation of a charge trap at lateral position $x_{\rm CT}$, defined in the lower inset.

$$\delta E_{ST_{\rm val(orb)}} \approx e|\langle T_{\rm val(orb)}|V_{\rm CT}|T_{\rm val(orb)}\rangle - \langle S|V_{\rm CT}|S\rangle|. \quad (6)$$

We note that interfacial disorder breaks the circular symmetry, allowing us to use nondegenerate perturbation theory for the circular confinement potentials used in this work. We evaluate Eq. (6) for the geometry shown in the lower inset of Fig. 3(c), that is typical for QDHQs, assuming a 10 nm Si quantum well, a SiGe barrier of width 40 nm, a 1 nm Si cap, a 5 nm layer of Al_2O_3, and a metal top gate. For simplicity, we consider the gate to be an infinite plane giving rise to a uniform electric field $\boldsymbol{F}^e$, but not the dot confinement potential. The dot confinement is simply given by Eq. (4), and we assume the image potentials for the dot electrons are subsumed into this potential. We take the charge trap to be located ~50 nm above the dot, inside the oxide layer, as suggested by recent experiments [42]. Because of its proximity to the top gate, the trap is strongly screened. Following Ref. [43], and using the dielectric constants of the different layers, we obtain the leading terms in the potential, $V_{\rm CT} \approx (1.13e/4\pi\epsilon_0\epsilon_r)(|\boldsymbol{R}-\boldsymbol{r}|^{-1} - |\boldsymbol{R}_{\rm im}-\boldsymbol{r}|^{-1})$, where $\boldsymbol{R}$ is the position of the trap, $\boldsymbol{R}_{\rm im}$ is the position of its mirror image inside the metal, and $\boldsymbol{r}$ is the position of the dot. To estimate the distance between the trap and the top gate, we consider a double-dot geometry with an interdot separation of 200 nm. The upper inset of Fig. 3(c) shows the shift $\delta\varepsilon$ in the double-dot detuning parameter ε, caused by a charge trap separated from the dot by a lateral distance $x_{\rm CT}$. Here, $x_{\rm CT} = 0$ corresponds to a charge trap located directly above the right dot. For a trap located 0.1 nm below the gate, the resulting shifts fall into the range $0-9$ μeV, as consistent with experimental measurements of detuning fluctuations σ_ε [40,44–47].

Our perturbative results for the dominant ST splittings are shown in Fig. 3(c), as obtained on either side of the triplet crossover, at locations $\hbar\omega = 550$ μeV ($ST_{\rm orb}$) or $\hbar\omega = 650$ μeV ($ST_{\rm val}$). As expected, the energy fluctuations are strongly suppressed for $ST_{\rm val}$. We can also estimate dephasing rates for QDHQ from the relation $\Gamma_2^* = (\sigma_\varepsilon/\sqrt{2}\hbar)|\partial E_Q/\partial\varepsilon|$ [20,48,49]. Assuming the charge trap has equal switching rates between its empty and occupied states, we can approximate the standard deviation of $E_{ST_{\rm val(orb)}}$ fluctuations as $(1/2)\delta E_{ST_{\rm val(orb)}}$, so that $\sigma_\varepsilon|\partial E_Q/\partial\varepsilon| \approx (1/2)\delta E_{ST_{\rm val(orb)}}$. Dephasing estimates obtained in this way are also reported in the main panel of Fig. 3(c). Here, we note that although, in general, semiconductor nanostructures are accepted to be subject to $1/f$ charge noise [50], recent experimental work suggests that some noise spectra in Si/SiGe devices are more consistent with an individual or a small number of defects [42]. For the settings considered here, we see that the dephasing rates for $ST_{\rm val}$ vs $ST_{\rm orb}$ can differ by a very large factor (~10), depending on the lateral position of the trap. The lower curve, associated with $E_{ST_{\rm val}}$, appears to be more consistent with recent experimental measurements of $\Gamma_2^* = 6$–210 MHz in a Si QDHQ [40],

lending support to the low-noise qubit design proposed here. We note that using valley vs orbital triplet states can have additional effects on qubit operation, unrelated to coherence. For example, they could affect the tunnel coupling, resulting in different gate times. If necessary, such changes may be compensated by tuning other devices' parameters, such as the confinement of the second dot, which would have little effect on qubit coherence. Finally, our results may also help to explain the much higher dephasing rates observed in a GaAs QDHQ [51], $\Gamma_2^* = 0.12$–1.4 GHz, which has no T_{val} state. (Note that the current results are obtained using Si materials parameters.)

Summary.—Using a combination of tight-binding and full-configuration-interaction calculations, we have shown that an important crossover occurs in the low-lying triplet state of two-electron dots in Si/SiGe: for weak confinement, the orbital triplet is the dominant excitation, while for strong confinement the valley triplet is dominant. We find that strong *e-e* interactions and valley-orbit coupling (induced by atomic steps at the quantum-well interface) both play key roles in this behavior, in the physically relevant operating regime. We further show that the charge distribution of the valley triplet is similar to that of the singlet, but differs from the orbital triplet. Consequently, qubits based on valley-triplet excitations are much more resilient to charge noise. These results are crucial for successful implementations of multielectron qubits in Si/SiGe dots, and also pertain to qubits formed in MOS systems for which valley splittings and confinement energies are typically higher than Si/SiGe systems [10,11].

We thank Mark Eriksson, J. P. Dodson, Joelle Corrigan, Tom McJunkin, Leah Tom, Merritt Losert, José Carlos Abadillo-Uriel, Mark Gyure, Samuel Quinn, Andrew Pan, Joseph Kerckhoff, Elliot Connors, and John Nichol for helpful discussions. This work was supported in part by ARO through Award No. W911NF-17-1-0274 and the Vannevar Bush Faculty Fellowship program sponsored by the Basic Research Office of the Assistant Secretary of Defense for Research and Engineering and funded by the Office of Naval Research through Grant No. N00014-15-1-0029. The views and conclusions contained in this document are those of the authors and should not be interpreted as representing the official policies, either expressed or implied, of the U.S. Government. The U.S. Government is authorized to reproduce and distribute reprints for Government purposes notwithstanding any copyright notation herein. This research was performed using the compute resources and assistance of the UW-Madison Center For High Throughput Computing (CHTC) in the Department of Computer Sciences. The CHTC is supported by UW-Madison, the Advanced Computing Initiative, the Wisconsin Alumni Research Foundation, the Wisconsin Institutes for Discovery, and the National Science Foundation, and is an active member of the Open Science Grid, which is supported by the National Science Foundation and the U.S. Department of Energy's Office of Science.

[1] E. Barnes, J. P. Kestner, N. T. T. Nguyen, and S. Das Sarma, Phys. Rev. B **84**, 235309 (2011).
[2] S. Mehl and D. P. DiVincenzo, Phys. Rev. B **88**, 161408(R) (2013).
[3] M. A. Bakker, S. Mehl, T. Hiltunen, A. Harju, and D. P. DiVincenzo, Phys. Rev. B **91**, 155425 (2015).
[4] T. Kodera, K. Ono, S. Amaha, Y. Arakawa, and S. Tarucha, J. Phys. Condens. Matter **150**, 022043 (2009).
[5] A. P. Higginbotham, F. Kuemmeth, M. P. Hanson, A. C. Gossard, and C. M. Marcus, Phys. Rev. Lett. **112**, 026801 (2014).
[6] B.-B. Chen, B.-C. Wang, G. Cao, H.-O. Li, M. Xiao, G.-C. Guo, H.-W. Jiang, X. Hu, and G.-P. Guo, Phys. Rev. B **95**, 035408 (2017).
[7] Z. Shi, C. B. Simmons, J. R. Prance, J. K. Gamble, T. S. Koh, Y.-P. Shim, X. Hu, D. E. Savage, M. G. Lagally, M. A. Eriksson, M. Friesen, and S. N. Coppersmith, Phys. Rev. Lett. **108**, 140503 (2012).
[8] D. Kim, Z. Shi, C. B. Simmons, D. R. Ward, J. R. Prance, T. S. Koh, J. K. Gamble, D. E. Savage, M. G. Lagally, M. Friesen, S. N. Coppersmith, and M. A. Eriksson, Nature (London) **511**, 70 (2014).
[9] P. Harvey-Collard, N. T. Jacobson, M. Rudolph, J. Dominguez, G. A. Ten Eyck, J. R. Wendt, T. Pluym, J. K. Gamble, M. P. Lilly, M. Pioro-Ladrière, and M. S. Carroll, Nat. Commun. **8**, 1029 (2017).
[10] R. C. C. Leon, C. H. Yang, J. C. C. Hwang, J. C. Lemyre, T. Tanttu, W. Huang, K. W. Chan, K. Y. Tan, F. E. Hudson, K. M. Itoh, A. Morello, A. Laucht, M. Pioro-Ladrière, A. Saraiva, and A. S. Dzurak, Nat. Commun. **11**, 797 (2020).
[11] C. H. Yang, R. C. C. Leon, J. C. C. Hwang, A. Saraiva, T. Tanttu, W. Huang, J. Camirand Lemyre, K. W. Chan, K. Y. Tan, F. E. Hudson, K. M. Itoh, A. Morello, M. Pioro-Ladrière, A. Laucht, and A. S. Dzurak, Nature (London) **580**, 350 (2020).
[12] L. Petit, H. G. J. Eenink, M. Russ, W. I. L. Lawrie, N. W. Hendrickx, S. G. J. Philips, J. S. Clarke, L. M. K. Vandersypen, and M. Veldhorst, Nature (London) **580**, 355 (2020).
[13] M. Friesen, S. Chutia, C. Tahan, and S. N. Coppersmith, Phys. Rev. B **75**, 115318 (2007).
[14] M. Friesen and S. N. Coppersmith, Phys. Rev. B **81**, 115324 (2010).
[15] M. D. Shulman, O. E. Dial, S. P. Harvey, H. Bluhm, V. Umansky, and A. Yacoby, Science **336**, 202 (2012).
[16] T. B. Boykin, G. Klimeck, M. A. Eriksson, M. Friesen, S. N. Coppersmith, P. von Allmen, F. Oyafuso, and S. Lee, Appl. Phys. Lett. **84**, 115 (2004).
[17] T. B. Boykin, G. Klimeck, M. Friesen, S. N. Coppersmith, P. von Allmen, F. Oyafuso, and S. Lee, Phys. Rev. B **70**, 165325 (2004).

[18] A. Szabó and N. Ostlund, *Modern Quantum Chemistry: Introduction to Advanced Electronic Structure Theory* (Macmillan, London, 1982).

[19] H. E. Ercan, S. N. Coppersmith, and M. Friesen, Phys. Rev. B **104**, 235302 (2021).

[20] J. C. Abadillo-Uriel, B. Thorgrimsson, D. Kim, L. W. Smith, C. B. Simmons, D. R. Ward, R. H. Foote, J. Corrigan, D. E. Savage, M. G. Lagally, M. J. Calderón, S. N. Coppersmith, M. A. Eriksson, and M. Friesen, Phys. Rev. B **98**, 165438 (2018).

[21] At this point, it is also possible to use more realistic potential profiles, based on self-consistent electrostatic methods, such as Thomas-Fermi [22] or Schrödinger-Poisson [23]; however, the underlying physics that we study here is not expected to depend on the exact form of the confinement potential.

[22] C. King, J. S. Schoenfield, M. J. Calderón, B. Koiller, A. Saraiva, X. Hu, H. W. Jiang, M. Friesen, and S. N. Coppersmith, Phys. Rev. B **101**, 155411 (2020).

[23] D. V. Melnikov and J.-P. Leburton, Phys. Rev. B **73**, 085320 (2006).

[24] R. A. Faulkner, Phys. Rev. **184**, 713 (1969).

[25] M. G. Borselli, R. S. Ross, A. A. Kiselev, E. T. Croke, K. S. Holabird, P. W. Deelman, L. D. Warren, I. Alvarado-Rodriguez, I. Milosavljevic, F. C. Ku, W. S. Wong, A. E. Schmitz, M. Sokolich, M. F. Gyure, and A. T. Hunter, Appl. Phys. Lett. **98**, 123118 (2011).

[26] X. Mi, C. G. Péterfalvi, G. Burkard, and J. R. Petta, Phys. Rev. Lett. **119**, 176803 (2017).

[27] J. S. Schoenfield, B. M. Freeman, and H. Jiang, Nat. Commun. **8**, 64 (2017).

[28] E. H. Chen, K. Raach, A. Pan, A. A. Kiselev, E. Acuna, J. Z. Blumoff, T. Brecht, M. D. Choi, W. Ha, D. R. Hulbert, M. P. Jura, T. E. Keating, R. Noah, B. Sun, B. J. Thomas, M. G. Borselli, C. A. C. Jackson, M. T. Rakher, and R. S. Ross, Phys. Rev. Applied **15**, 044033 (2021).

[29] D. M. Zajac, T. M. Hazard, X. Mi, E. Nielsen, and J. R. Petta, Phys. Rev. Applied **6**, 054013 (2016).

[30] J. P. Dodson, H. Ekmel Ercan, J. Corrigan, M. Losert, N. Holman, T. McJunkin, L. F. Edge, M. Friesen, S. N. Coppersmith, and M. A. Eriksson, Phys. Rev. Lett. **128**, 146802 (2022).

[31] J. Corrigan, J. P. Dodson, H. E. Ercan, J. C. Abadillo-Uriel, B. Thorgrimsson, T. J. Knapp, N. Holman, T. McJunkin, S. F. Neyens, E. R. MacQuarrie, R. H. Foote, L. F. Edge, M. Friesen, S. N. Coppersmith, and M. A. Eriksson, Phys. Rev. Lett. **127**, 127701 (2021).

[32] G. W. Bryant, Phys. Rev. Lett. **59**, 1140 (1987).

[33] C. Yannouleas and U. Landman, Phys. Rev. Lett. **82**, 5325 (1999).

[34] R. Egger, W. Häusler, C. H. Mak, and H. Grabert, Phys. Rev. Lett. **82**, 3320 (1999).

[35] A. V. Filinov, M. Bonitz, and Y. E. Lozovik, Phys. Rev. Lett. **86**, 3851 (2001).

[36] B. Reusch, W. Häusler, and H. Grabert, Phys. Rev. B **63**, 113313 (2001).

[37] See Supplemental Material at http://link.aps.org/supplemental/10.1103/PhysRevLett.128.247701 for a discussion of interface profiles that give small *ST* splittings.

[38] D. Culcer, A. L. Saraiva, B. Koiller, X. Hu, and S. Das Sarma, Phys. Rev. Lett. **108**, 126804 (2012).

[39] N. E. Penthorn, J. S. Schoenfield, J. D. Rooney, L. F. Edge, and H. Jiang, npj Quantum Inf. **5**, 94 (2019).

[40] B. Thorgrimsson, D. Kim, Y.-C. Yang, L. W. Smith, C. B. Simmons, D. R. Ward, R. H. Foote, J. Corrigan, D. E. Savage, M. G. Lagally, M. Friesen, S. N. Coppersmith, and M. A. Eriksson, npj Quantum Inf. **3**, 32 (2017).

[41] J. K. Gamble, M. Friesen, S. N. Coppersmith, and X. Hu, Phys. Rev. B **86**, 035302 (2012).

[42] E. J. Connors, J. J. Nelson, H. Qiao, L. F. Edge, and J. M. Nichol, Phys. Rev. B **100**, 165305 (2019).

[43] T. Takashima and R. Ishibashi, IEEE Trans. Electr. Insul. **EI-13**, 37 (1978).

[44] X. Wu, D. R. Ward, J. R. Prance, D. Kim, J. K. Gamble, R. T. Mohr, Z. Shi, D. E. Savage, M. G. Lagally, M. Friesen, S. N. Coppersmith, and M. A. Eriksson, Proc. Natl. Acad. Sci. U.S.A. **111**, 11938 (2014).

[45] X. Mi, S. Kohler, and J. R. Petta, Phys. Rev. B **98**, 161404 (R) (2018).

[46] T. F. Watson, S. G. J. Philips, E. Kawakami, D. R. Ward, P. Scarlino, M. Veldhorst, D. E. Savage, M. G. Lagally, M. Friesen, S. N. Coppersmith, M. A. Eriksson, and L. M. K. Vandersypen, Nature (London) **555**, 633 (2018).

[47] L. Kranz, S. K. Gorman, B. Thorgrimsson, Y. He, D. Keith, J. G. Keizer, and M. Y. Simmons, Adv. Mater. **32**, 2003361 (2020).

[48] O. E. Dial, M. D. Shulman, S. P. Harvey, H. Bluhm, V. Umansky, and A. Yacoby, Phys. Rev. Lett. **110**, 146804 (2013).

[49] K. D. Petersson, J. R. Petta, H. Lu, and A. C. Gossard, Phys. Rev. Lett. **105**, 246804 (2010).

[50] P. Huang and X. Hu, Phys. Rev. B **89**, 195302 (2014).

[51] G. Cao, H.-O. Li, G.-D. Yu, B.-C. Wang, B.-B. Chen, X.-X. Song, M. Xiao, G.-C. Guo, H.-W. Jiang, X. Hu, and G.-P. Guo, Phys. Rev. Lett. **116**, 086801 (2016).